Handling Dataset with Geophysical and Geological Variables on the Bolivian Andes by the GMT Scripts

Polina Lemenkova

data

MDPI

Article

Handling Dataset with Geophysical and Geological Variables on the Bolivian Andes by the GMT Scripts

Polina Lemenkova

Laboratory of Image Synthesis and Analysis, École Polytechnique de Bruxelles, Université Libre de Bruxelles, 1050 Brussels, Belgium; polina.lemenkova@ulb.be or pauline.lemenkova@gmail.com; Tel.: +32-471860459

Abstract: In this paper, an integrated mapping of the georeferenced data is presented using the QGIS and GMT scripting tool set. The study area encompasses the Bolivian Andes, South America, notable for complex geophysical and geological parameters and high seismicity. A data integration was performed for a detailed analysis of the geophysical and geological setting. The data included the raster and vector datasets captured from the open sources: the IRIS seismic data (2015 to 2021), geophysical data from satellite-derived gravity grids based on CryoSat, topographic GEBCO data, geoid undulation data from EGM-2008, and geological georeferences' vector data from the USGS. The techniques of data processing included quantitative and qualitative evaluation of the seismicity and geophysical setting in Bolivia. The result includes a series of thematic maps on the Bolivian Andes. Based on the data analysis, the western region was identified as the most seismically endangered area in Bolivia with a high risk of earthquake hazards in Cordillera Occidental, followed by Altiplano and Cordillera Real. The earthquake magnitude here ranges from 1.8 to 7.6. The data analysis shows a tight correlation between the gravity, geophysics, and topography in the Bolivian Andes. The cartographic scripts used for processing data in GMT are available in the author's public GitHub repository in open-access with the provided link. The utility of scripting cartographic techniques for geophysical and topographic data processing combined with GIS spatial evaluation of the geological data supported automated mapping, which has applicability for risk assessment and geological hazard mapping of the Bolivian Andes, South America.

Keywords: cartography; spatial data; GIS; georeferencing; mapping; Bolivia; Latin America; geodesy

Citation: Lemenkova, P. Handling Dataset with Geophysical and Geological Variables on the Bolivian Andes by the GMT Scripts. *Data* **2022**, 7, 74. https://doi.org/10.3390/data7060074

Academic Editors: Vladimir Sreckovic, Milan S. Dimitrijević and Zoran Mijic

Received: 15 April 2022
Accepted: 30 May 2022
Published: 1 June 2022

1. Introduction

1.1. Background

For many problems in Earth sciences, cartographic datasets are the key sources for spatial analysis and visualisation. Spatial data have a great potential for many applications in various fields, such as geophysics, geology, and the environment. However, the most important issue in the mapping workflow consists of finding the effective algorithms of processing the multi-source and heterogeneous spatial data. In this paper, the integrated use of the techniques of the Geographic Information System (GIS) and the Generic Mapping Tools' (GMTs) cartographic scripting tool set for processing geospatial data is proposed.

Spatial data include two major types of format, often used in a mapping workflow: raster and vector. The fundamental differences in their structure entail various means of their handling and processing. The use of scripts for processing cartographic data brings significant improvements to the mapping process [1–5]. Examples of such applications include the modules of GMT for cartographic tasks of data visualisation. Effective processing of geospatial data by scripts is especially important for large datasets with global Earth coverage [6–9]. The console-based data processing using scripts enables increasing the accuracy and speed of data processing in cartographic analysis and plotting. Therefore, using advanced geospatial software and tools is also of major importance in many GIS-related applications that include geospatial data processing, e.g., machine learning in GIS [10–14],

data retrieval, exploration and processing [15–17], spatial data formatting, handling and compression [18–21], and geographic data modelling and analysis [22–24].

Raster data and images are often derived from remote sensing (RS) sources such as satellite images. Examples of using raster data in geographic studies include satellite imagery, for instance Sentinel-1 and 2A, used for mapping the high-resolution spatio-temporal dynamics of land use and land cover [25,26]. The wide use of the Landsat TM/ETM+ by ESA for geological and land cover mapping is explained by data availability and global coverage [27–29]. The aerial Google Earth or the commercial geospatial data providers operating of large-scale aerial data for detailed mapping. More examples of raster data sources include hyperspectral imagery, InSAR largely used in geology [30,31], or LiDAR used for geomorphic computations or vegetation canopy height [32,33]. Important data sources for topographic mapping are derived from the SRTM DEM.

Using raster data as a source of information are often a case for land cover mapping and landscape analysis [34–36]. Scanned raster images in bitmap formats (jpg, bmp, tiff) provide another source of information aimed at retrospective data analysis for geospatial reconstructions [37,38]. Used as georeferenced raster layers in GIS, archived historical maps can be utilised as data sources for evaluating landscape dynamics and serve as an auxiliary source for geologic analysis and mineral resource management. Technically, processing raster data is based on the analysis of pixels on the image and, if necessary, the steps of vectorisation [39–41]. In the advanced cases, the RS data can be processed using machine learning techniques.

Vector data, on the other hand, are often used to represent geographical information on the object-based level [42,43]. The information containing ontologies of vector data is included in the attribute tables of the associated GIS tables or the metadata of the layers [44]. Vector data sources include, e.g., the vectorised objects as georeferenced layers in GIS formats (e.g., .shp format of ArcGIS/QGIS). The integration and complementary use of vector and raster data can be applied in cadastral cartography and LiDAR altimetric data, providing information for the 3D vector-based models [45]. A special feature of vector data consists of the object-based structure, which entails points, lines, or polygons formed by a variety of curves or points with coordinates in a spatial reference format. Thus, vector objects indicate the boundaries or depict the contours of geographic objects varying in geometry, form, size, shape, curvature, connectivity, and spatial resolution, which depend on the map scale [46].

1.2. Study Objectives

This article presents an integrative data-driven cartographic synthesis technique that enables processing vector geological data and raster geophysical data, while exploring all the advantages of GIS and GMT applied in one framework. Although existing GISs for geospatial data processing are widely available, directly using their functionality does not offer an intuitive, direct control on data handling as in the case of using scripts. In fact, various GIS software often provide the designed solutions for mapping the workflow. In contrast, the script-based technique provides more control on data processing.

This study is focused on processing spatial data for cartographic visualisation using geological, topographic, and geophysical datasets for Bolivia (Figure 1). The integration of the vector and raster data in a structured way by means of various technical tools supports the increase of geographical and expert knowledge. Creating such a project with a special focus on the Bolivian Andes is built upon the data captured from the available open sources. The study framework is designed to visualise the multi-sources data of various formats. The presented series of maps is aimed at contributing to monitoring natural resources in a selected region of the geographically complex region of South America.

Figure 1. Topographic map of the study area. Visualisation: GMT. Source: author.

2. Materials and Methods

Methods of GIS mapping and geoinformatics passed several epochs from their onset in the 1970s, including rapid development of computer technologies and progress in spatial data standards and formats. Besides, the approaches related to remote sensing, Earth observation, and geological data processing largely use spatial data [27,47,48]. Although these approaches have advantages in geospatial data processing, those methods are not efficient enough for processing large datasets in real time, which requires machine-based cartographic data visualisation. Currently, the contemporary methods of spatial data processing include a high degree of computing and scripting with the recent application of machine learning, scripting, and programming in geosciences [49–52].

The current study aimed to identify the distribution and magnitude of earthquakes in the Bolivian Andes in the context of the geologic, geophysical, and topographic situation. The study was performed using the technical integration of QGIS and GMT scripting tools applied to Bolivia. The topographic elevation data, geologic provinces and units, as well as seismic events obtained from the IRIS database were mapped. The five full scripts used in this study for GMT mapping are available in the GitHub repository of the author with public open-access: https://github.com/paulinelemenkova/Mapping_Bolivia_GMT_Scripts (accessed on 31

May 2022). The topographic map (Figure 1) was mapped as a background for the IRIS seismic data. It was derived from the General Bathymetric Chart of the Oceans (GEBCO) gridded bathymetry and topography dataset [53]. The GEBCO presents consistent and accurate digital elevation data covering the Earth, largely used in the Earth sciences as a reliable data source. The unprecedentedly high resolution (15 arc second) of the GEBCO grid enables using it as a fine cartographic grid both for topographic mapping and as a background for the overlaying thematic maps [54].

The EGM-2008 [55] digital geoid model was used to show variations in gravity over the territory of Bolivia that correlate with the topographic map. A general increase of gravity values is notable in the southwest direction, which coincides well with the geographic extent of the Central Andes. The data on gravity were obtained from the repositories of Scripps Institution of Oceanography [56]. The IRIS database of the world's seismicity was applied for Bolivia for the period of 2015–2021. It was used to map the earthquake events recorded in the Central Andes for the six-year time span. Several columns of the initial table in CSV format presented seismic parameters of the earthquakes (depth and magnitude), the coordinates and time of the event (date-month-years), a brief description, and the location. The table recording 3000 seismic events in Bolivia was converted from CSV to the NGDC format for plotting in GMT. The study employed existing GIS methods [16,57–61] and presents the two geologic maps made using the QGIS software [62].

Besides the GIS, the study applied the GMT, developed and continuously maintained by [63]. In contrast to the traditional GIS, the GMT refers to a console-based scripting framework aimed at automated and effective plotting of the geospatial data. The cartographic approach of GMT enables effective mapping and data visualisation, based on shell scripting [64,65]. It includes a variety of data processing steps, such as conversion, reshaping, reformatting, modelling, spatial analysis, and visualisation. The process of GMT mapping was adapted in this work based on the previous existing studies [66].

3. Study Area

Identifying the correlations between the geological structure, topography, and geophysics and seismicity gives better insights into our understanding of the geological hazards and risk assessment in the mountainous regions shown in previous works [10,67–69]. The study object is presented by the Bolivian segment of the Andes Mountains. The Andes Mountains present a unique geologic, geomorphological, and tectonic structure built upon the thickest crust on Earth. The Andes are the longest continental mountain range stretching along the western margins of South America and crossing several countries including Bolivia (Figure 1).

The Andes are the key geological object of Bolivia directly affected by their tectonic history. The geological evolution of the Bolivian segment of the Andes has underwent a long multi-stage period of formation, which has been reported and described in detail in previous studies [70,71] and in some earlier fundamental books on South American geology [72–74]. Bolivia occupies the Central Andes segment with Altiplano, the world's 2nd highest mountain plateau after Tibet. The tectonics of the Andes largely controls the geomorphology of the Bolivian mountainous lakes (shape, orientation, and geometry), primarily by a nearly orthogonal fracture pattern from the underlying granitic basement (Brazilian Shield) and, secondarily, by the tectonic movements: ancient global fracture pattern, principal compressive stress, downwarping and uplifting of the Beni Basin during the Cenozoic Andean orogeny [75].

The geologic setting of the Central Andes (Figures 2 and 3) have been previously described in earlier works by many researchers [76–78]. The specific features of the Central Andes have drawn the attention of Earth scientists in various disciplines, e.g., hydrogeologists [79,80], geophysicists [81,82], and seismologists [83,84]. The historic evolution of the Bolivian Andes underwent several stages during the early history of the Earth. Among the notable geologic events of Bolivia is the San Ignacio Orogeny, which reshaped the terrane through the deformations accompanied by the voluminous tectonic granite intrusions and deformations of the sediments [85].

The dominating units in central Bolivia (Figure 2) are presented by the Cambrian-Ordovician (CmO) outcrops, which largely contrast with a very complex disposition of several layers in the west of the country in the Central Andes region: Ordovician-Silurian (OS), Devonian (D), Silurian (S), Tertiary (T), and Cretaceous-Tertiary volcanics (Cv).

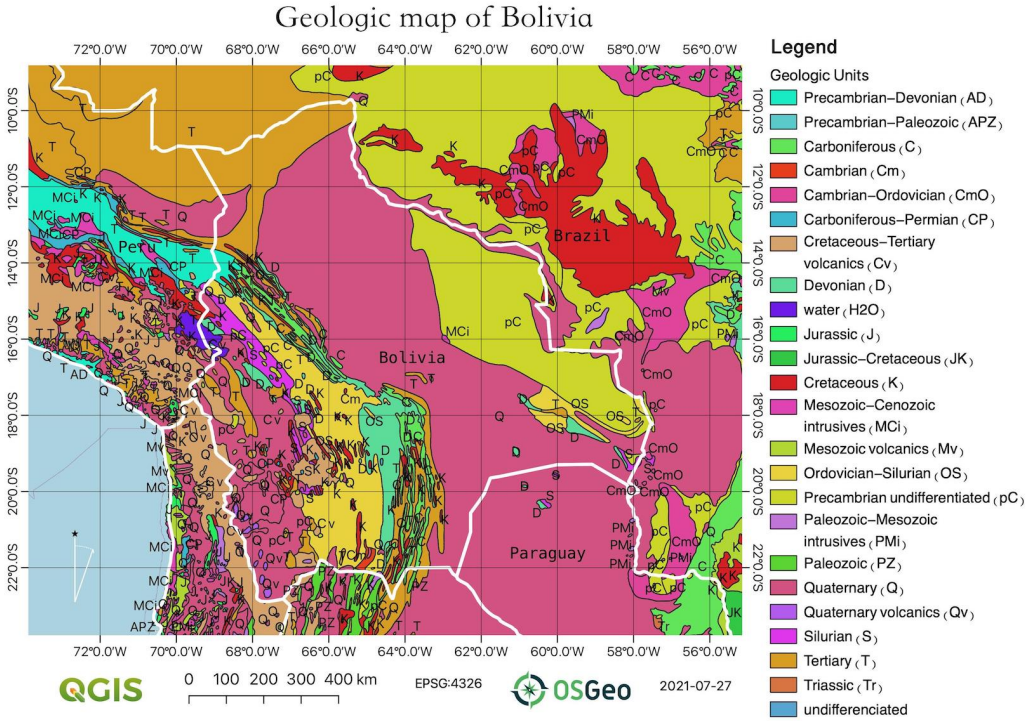

Figure 2. Geologic map of Bolivia and surrounding countries. Visualisation: QGIS. Source: author.

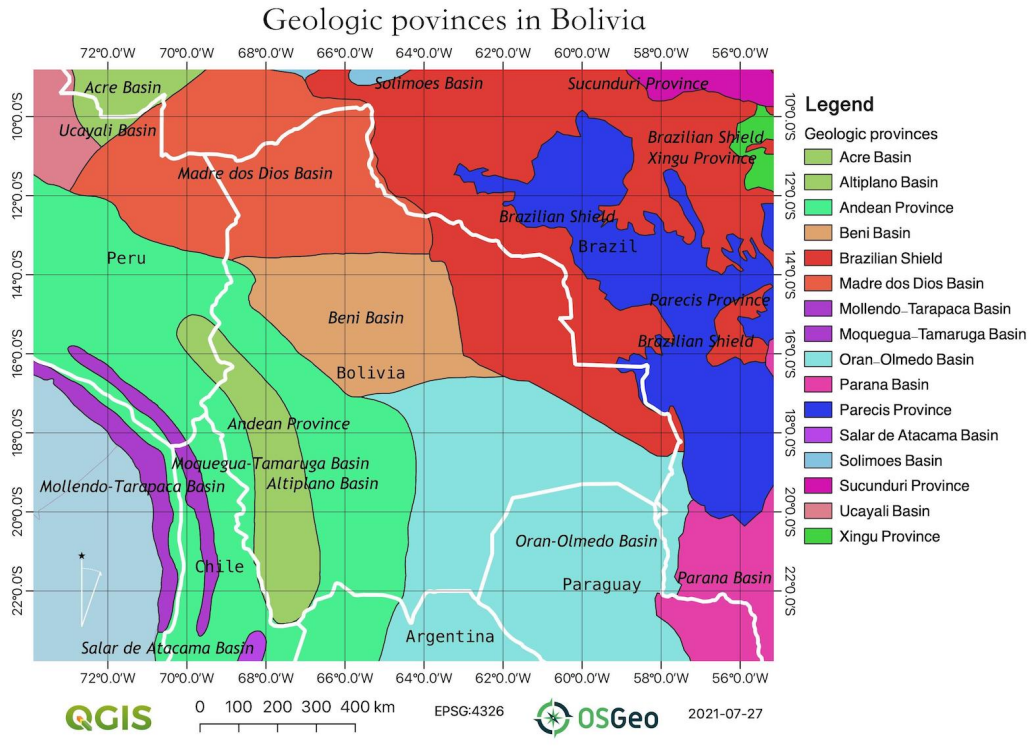

Figure 3. Geologic provinces in Bolivia and surroundings. Visualisation: QGIS. Source: author.

The eastern part of the country, presented by the Amazon forests, is occupied by the Precambrian outcrops (pC), which well correspond to the extent of the Brazilian Shield (Figure 2). The geological structures of the Bolivian orogeny are generally oriented in the NW direction off Amazonia, following the extent of the Central Andes. The Andes act as a source of precious mineral and geological resources in Bolivia. This is caused by the intensive tectonic processes and orogenesis in the past, which took place in these geological provinces (Figure 3).

The most important geological provinces of Bolivia include the Madre dos Dios in the north, mostly covered by the Tertiary rocks (T), the Brazilian Shield to the east, the Oran-Olmedo Basin to the south (covered by the Cambrian-Ordovician outcrops), the Beni Basin in the central-northern segment of the country, and the Andean Province to the west (covering the Central Andes) with the intrusion of the Altiplano Basin. The formation of precious metals in the Andes includes a system of complex petrographic and geochemical processes that result in the evolution of magmas and lavas that underwent fractionation and assimilation in the Earth's crust [86]. As a result, the mining industry has had a dominant position in the country's economy since the 16th Century. As a result, Bolivia holds a leading position in the reserves of tin, zinc, silver, copper, gold, tungsten, lead, and antimony [87–90]. Besides, the Bolivian Salar de Uyuni salt flat is the world's largest lithium deposit [91,92].

The regional geomorphology of the Andes affects a wide variety of the interconnected processes in Bolivia linking hydrology, environment, soils, ecology, climate, and landscapes. For instance, the tectonic faults, lineaments, and structure of the underlying rocks cause variations in the geomorphic and hydrological fluvial structure of the country. This was recorded within the drainage network of the Andean foreland, which is preserved in the palaeochannels of the Bolivian Amazon, varying in sinuosity, width, and the pattern of the Amazon rivers [93]. The types of landscapes of Bolivia vary according to their specific location within the Andes, which serve as a natural barrier to the air masses controlling climate though fluctuations in temperature, humidity, and water balance.

The geomorphological patterns initially formed by the geological processes are mirrored in fluvial belts, lacustrine patterns, and riverine meanders in Bolivia and shaped the landscapes of the country [94]. The landscapes in eastern Bolivia located along the southern margin of the Amazon basin are largely affected by climate through the strong hydrological and climatic seasonality, e.g., high wind speeds and aeolian processes. This affects the geomorphology and the environment of the eastern part of the country, forming special aeolian landforms, such as linear sand streaks and ridges, parabolic and elongate morphological structures, dunes, sand sheets, and mega-ripples. Hence, climate and aeolian processes largely control the environmental, vegetation, and soil setting in the country [95].

Various regions of the Bolivian Andes give place to the National Parks and protected nature conservation zones [96–98]. Besides the mountainous regions, the forests of the Bolivian Amazon provide the ecological habitat for endemic species [99], which demonstrates the environmental significance of this region. Besides the climatic and geologic factors affecting the landscapes, landscape changes in Bolivia are also influenced by anthropogenic activities. For example, according to the study in the Iroco and Cueva Bautista regions in the highlands of Bolivia, human settlements in the high-altitude ecosystems (>3800 m asl) occurred, at least, by 13,000 years BP [100].

At the same time, the seismicity of the Andes is high with repetitive earthquakes of various focal depth, rupture size, and magnitude [101,102]. In turn, earthquakes are closely associated with tectonic activity and zones of plate subduction. Magma evolution and assimilation at the subduction zones of the Andes significantly affected the geologic setting in South America in the past [103,104]. The earthquakes usually have negative consequences and involve such hazardous events as landslides, rockfalls, and ground shaking. This leads to damaged and destroyed buildings, ruined bridges and other constructions, losses in economics and financial instability, and in the worst cases, affected or lost human lives. The possibility of geologic

hazards in the mountainous regions of the Central Andes resulted in intensive geological investigations of Bolivia, as reported in earlier studies [105–108].

4. Results

In the present study, the geophysical and geological maps of Bolivia were created for comparison with the seismicity, topography, and geomorphological variability.

The topography of Bolivia (Figure 1) shows regional variations that well reflect the Quaternary geologic history, including the periods of glaciations in the high mountains of the Bolivian Andes during the Pleistocene, e.g., the Cordillera Real [109]. The glaciation in the Bolivian Andes experienced several periods in its early geologic history. These include the Tertiary and Early Pleistocene (>790 ka), Middle Pleistocene (790–132 ka), Late Pleistocene (132–11.7 ka), and Holocene (11.7 ka) [110]. The results of these glaciations remained as a system of the bedded slope deposits on the moraine ridges in the Bolivian Andes. The Late Pleistocene glaciations also formed the megafans of the Gran Chaco—a huge plain in eastern Bolivia which presents the main biogeographic biome of South America.

The contrasting glaciation formed a series of large piedmont fans of the Andes that were developed during the colder and seasonal conditions and dry–wet intense seasons and enhanced rainfalls by the orographic effects of the Andes [111,112]. A complex interrelation of the vegetation, climate, and soils can be illustrated by the reduced forest cover due to the increased aridity in the selected landscapes, soil formation, and intensive sedimentation in the dense forest cover in the Bolivian Chaco [113]. Besides glaciation, external factors that strongly affected the topography of Bolivia include the fluvial and aeolian interactions, the climate, and biogeographic effects. These mostly formed the Gran Chaco and selected regions of Amazonia through the distribution of the subtropical semi-deciduous vegetation and associated specific soil types in the piedmonts of the Andes.

The geologic maps (Figures 2 and 3) reflect the current state of the processes of solid Earth physics in the Andes. Thus, the metamorphic rocks and outcrops of various geologic epochs experienced solid-state mineral transformations due to changes in pressure and temperature in the crust and mantle of the Earth and record the geological periods, heating, seismic processes, and cooling, which in turn, reflect the tectonic processes they were formed in [114]. As a result, a complex geological history of the Bolivian Andes reflects its regional geology and petrographic setting, as well as the origin, distribution, and geochemistry of the minerals [115].

Regional undulations of the geoid (Figure 4) well correlate with the topography. For instance, the values of the geoid increase westward exceeding 34 m, which well correlates with the geomorphology of the Central Andes. In general, the isolines increase towards the west of Bolivia. In contrast, negative values of the geoid (from 10 to −10) are visible in the NE region and mostly cover the Amazon region of Brazil. The Beni Basin of Bolivia (Figure 3) demonstrates a slight decrease in data (from 20 to 16 m), while central regions of the Madre dos Dios Basin show a local increase in the geoid values (up to 32 m in the surroundings of Madidi National Park).

The comparison of the geological map in Figure 2 with the geoid in Figure 4 shows a distinct correlation between these two. The distribution of the geologic folds situated westward off the Cambrian-Ordovician outcrops well repeats the dense and steep increase in the isolines of the geoid detecting the increase of the gravity, which in turn, well correlates with the extent of the mountain areas of the Andes (red colour areas in Figure 4 show values of the geoid over 35 m). The correlation in changes of the free-air gravity (Figure 5) and vertical gravity gradient (Figure 6) with the topography (Figure 1) and geologic setting (Figure 2) are found by the comparison of these maps, further from the Andes to the Amazonia area and the Gran Chaco region.

The analysis of the values of the free-air gravity (Figure 5) and vertical gravity (Figure 6) demonstrates a very good correlation with the local lacustrine and riverine depressions of the mountainous lakes in Bolivia (Laguna Rogagua, Laguna San Luis), the rivers of Amazonia, the regional depression of the Gran Chaco on the border with Paraguay, and the piedmonts of the Andes (dark blue colours in Figures 5 and 6). In contrast, the highest

elevation peaks of the Bolivian Andes (Cordillera Real, Cordillera Occidental, and Altiplano) well correlate with the highest values in the geophysical data. The correlation of the gravity data with the geoid (Figure 4) well exhibits the lowest geoid values in the regions of the lower gravity in Figures 5 and 6 and the saddle-like local depression in the region of the city La Santísima Trinidad (central Bolivia), showing local topographic depression.

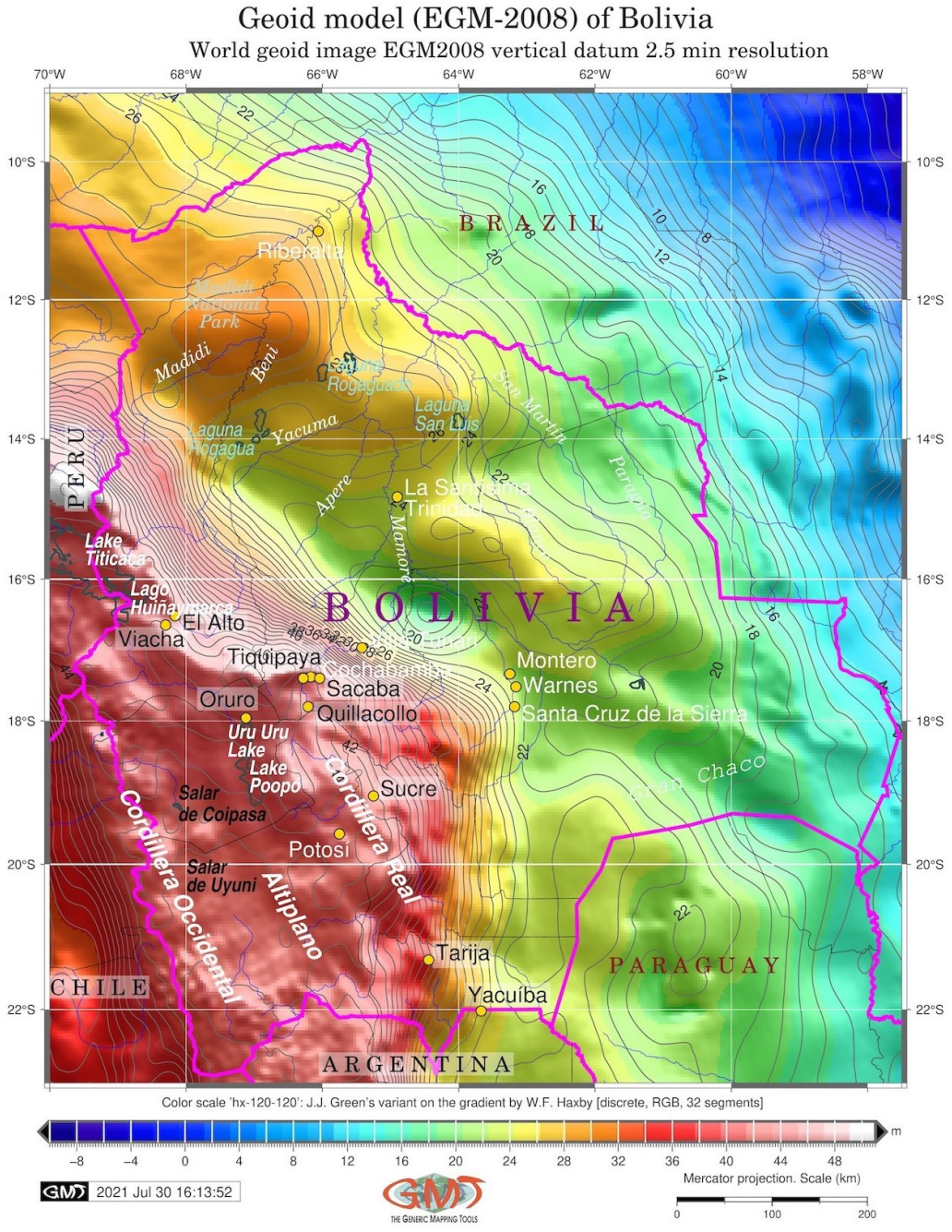

Figure 4. Geoid model of Bolivia. Visualisation: GMT. Source: author.

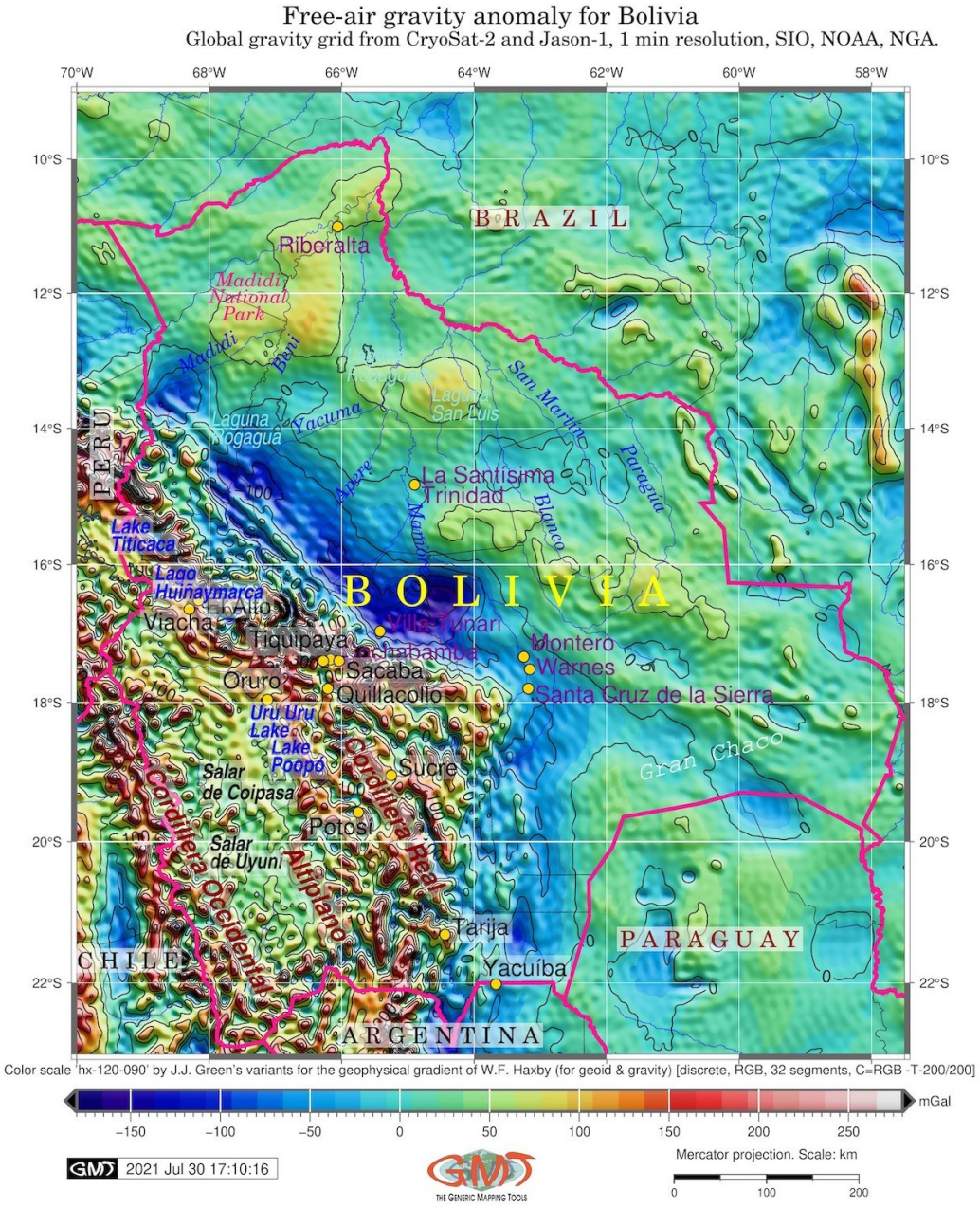

Figure 5. Free-air gravity map of Bolivia. Visualisation: GMT. Source: author.

The overall distribution of the earthquakes in Bolivia (Figure 7) indicate a good correlation with the geological extent of Cordillera Occidental, followed by Altiplano and Cordillera Real. In total, 3000 records have been assessed using the IRIS database for the period of 2015–2021. In general, the higher seismicity level of Bolivia is clearly visible in the westernmost region of the country. The earthquake with the least moment magnitude (1.8) was detected 17 km ESE of the Iquique, Chile, at a depth of 20 km. In contrast, the most significant, very deep earthquake events are located 211 km S of Tarauaca, Brazil (620.6 km, moment magnitude 7.6), and at 173 km WNW of Iberia, Peru, with a depth of 606.2 km. In the inner western region of the Andes (Cordillera Occidental), a series of volcanoes were mapped (Figure 7), to show a correlation with a higher magnitude of earthquakes (M 3.4 to 4.0 and 4.1 to 4.7).

The most significant earthquake in Bolivia was located 11 km NNE of Carandayti with a depth of 559 km and a moment magnitude of 6.8. Furthermore, some significant

earthquakes within the strongest magnitude (above 7) were located in Peru: (1) 140 km WNW of Iberia, Peru, which took place in 2018 with a moment magnitude of 7.1 at a depth of 630 km; (2) 38 km SSW of Acari, Peru, also dated 2018, with a moment magnitude of 7.1 located at a depth of 39 km (shallow earthquake). Thus, one can conclude that the most significant earthquake during the last 6 years (2015–2021) in Bolivia did not exceed a moment magnitude of 7.0, which indicates a rather lower seismic activity in Bolivia and less risk to the population, if compared, for example, to Peru.

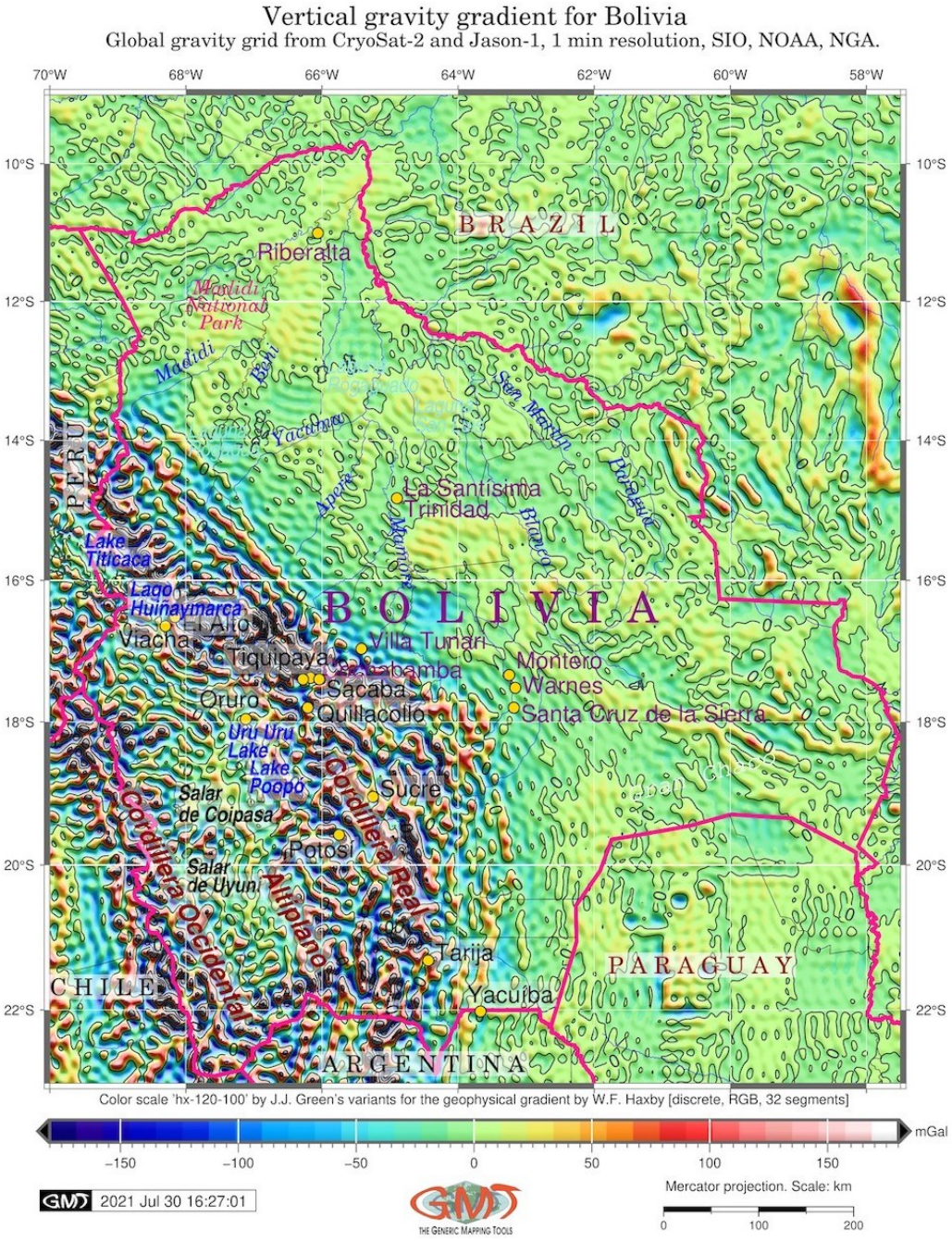

Figure 6. Vertical gravity gradient in Bolivia. Visualisation: GMT. Source: author.

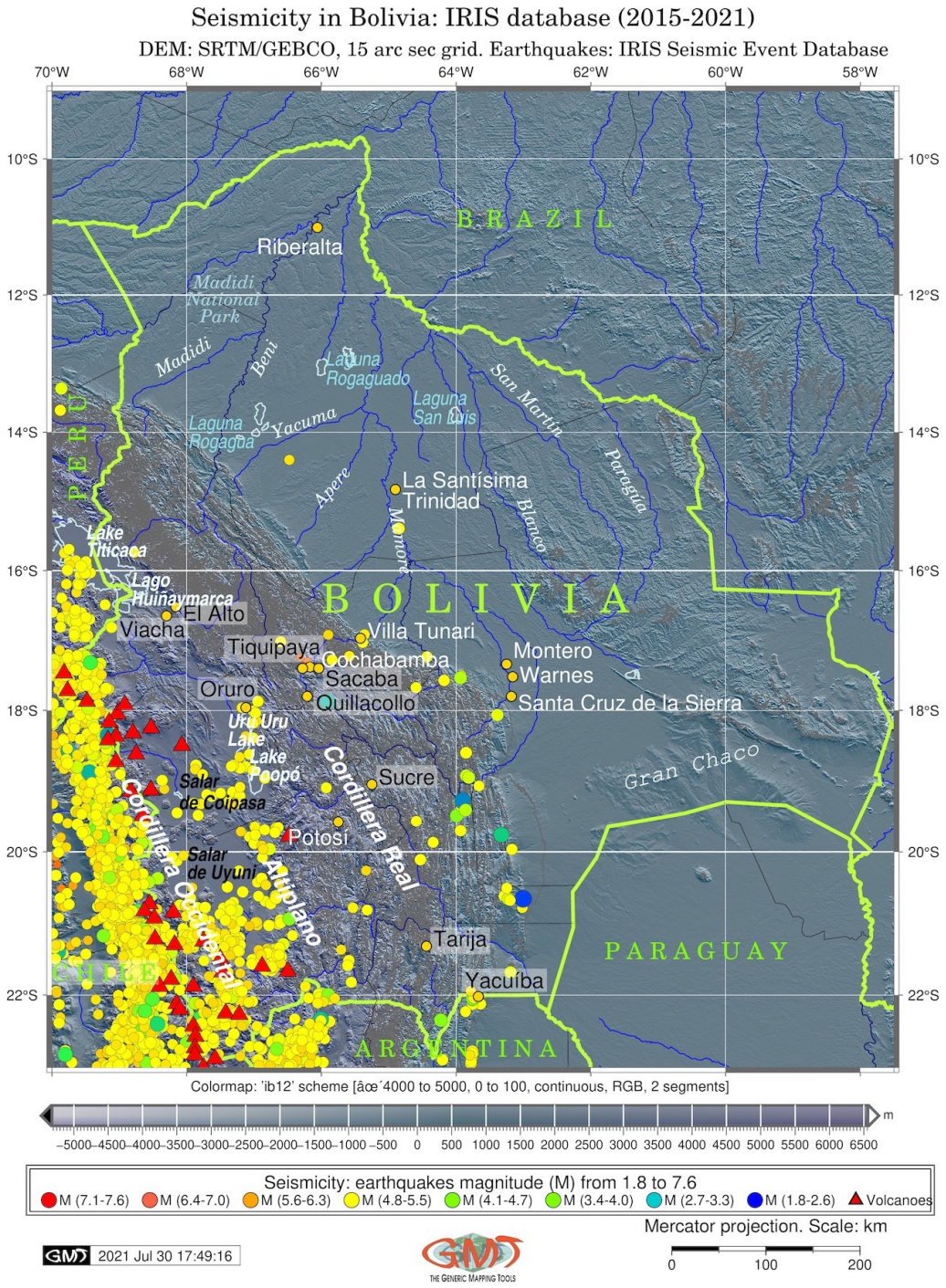

Figure 7. Seismicity in Bolivia and the Central Andes. Visualisation: GMT. Source: author.

5. Discussion

Using scripting techniques of GMT has many applications in geosciences, for example the analysis of the geologic setting of the Earth, climate modelling, exploring the atmosphere–ocean–solid earth interactions, which require advanced mapping, and many more. Rapid processing of maps by GMT enables producing a series of maps, which is a crucial source of geo-information for such tasks. To fully utilise the potential of GMT, the abilities and advantages of the modern scripting approaches should be used. In this research, I demonstrated the functionality of GMT and QGIS for the thematic mapping of the Andes region using the geological and geophysical datasets available from the open sources.

Currently, the geo-information data are available online in many sources, which increases the need for rapid and robust processing of these data, based on the availability.

To this end, a data-driven approach of GMT and QGIS was introduced in this paper for the thematic geological–geophysical mapping of the Andes region, Bolivia. Using the functionality of this program, this paper presented a workflow where I showed that it performs well on cartographic data processing without the manual tedious workflow usually applied in cartography. The geological features of regional objects in the Andes were mapped to show geological structure of Bolivia.

The most important geological units were mapped to show the outcrops of various geologic time: Precambrian-Devonian, Palaeozoic, Carboniferous, Cambrian, Ordovician, Permian, Tertiary Jurassic, Mesozoic, Cenozoic, Silurian, Triassic, and Quaternary as the major units. The algorithms of GMT processed well relatively large files (each raster file mapped for visualisation of the geoid, gravity, and seismicity has a size of several hundreds of MB) and converted these data into GMT native format for processing. Some complex regions of seismicity with overlapped sources of earthquakes were visualised using various colours and sizes of legend units for a better interpretation. Graphical representations of the maps were illustrated in relevant sections.

Mapping multi-source geo-information data are based on the processing and visualising of relevant thematic layers showing the geological and geophysical features of the target objects, such as free-air gravity anomalies, vertical gravity gradients, earthquakes, and other concepts. The major principle of GMT consists of creating the lines of code based on its syntax language. For instance, the projection and selected colour palettes were set up experimentally for each corresponding geographic phenomenon to better show the variations in levels. Such adjustments enabled better indicating the correlations between the topography and geophysics of the Andes region.

Moreover, the integrated use of the techniques of QGIS and GMT was used to identify the relationships between the geological and geophysical phenomena of the Earth through the prepared maps. Based on the setup parameters of GMT, a series of maps was created using a machine-based approach using scripts run from the console. A step-by-step cartographic process applied for the presented maps is shown in the scripts available in the GitHub repository with the provided link.

This workflow arrived at the data processing and visualisation on the presented series of maps showing the geologic, geophysical, and topographic features of Bolivia. However, certain steps in a cartographic workflow require manual adjusting and improvements in QGIS compared to GMT, which demonstrates a higher level of automation in the spatial data processing of the latter. The most geologically complicated regions (folds in the Bolivian Andes) were mapped using the enlarged zoom, to gain more insights into the visual characteristics of the small areas (e.g.,see the Devonian and Ordovician outcrops in Figure 2), as well as to discriminate the strata from the undifferentiated areas. To do so, I enlarged the selected areas on the map and controlled the visualisation manually using a zoom function of QGIS. Specifically, I identified the densely interspersed outcrops of the Cretaceous-Tertiary volcanics (Cv), Precambrian-Devonian (AD), and Palaeozoic (PZ) units in the Bolivian Andes, which demonstrated a distinct correlation between the gravity anomaly and the topographic heights of the same territory.

This study presented an integrated application of the GMT scripting tool set and the QGIS software used for mapping the geological and geophysical features of Bolivia in a semi-automatic regime in GMT and a manual approach in QGIS. I noted that while using a reliable software tool is a major task of any cartographic workflow, there are still more algorithms that need to be adjusted in GMT for a more automated cartographic workflow. Processing geo-information is an essential part of geophysical and geological research, having its specifics compared to the topographic or environmental mapping: the interpretation of the geophysical anomalous fields, visualising seismic events as a series of earthquakes with different magnitudes and depths, detecting geoid undulations using isoline directions and interpretation, and smooth data conversion from the seismic IRIS

catalogue into GMT, to mention a few of such tasks. This paper presented an example of such a study showing the integrated use of GMT and QGIS for processing the geological, topographic and geophysical data with the special example of Bolivia, South America.

6. Conclusions

In this study, a data-driven cartographic approach for data processing was presented using an example of scripting techniques of GMT applied for raster-based data and GIS-based mapping for vector data. By exploring the principles of the console-based mapping in GMT, this study visualised and evaluated the geophysical parameters that capture the intrinsic geologic properties of the Bolivian Andes, as demonstrated through the existing links on a series of maps. The study also used the modular technique of GMT to increase the speed, accuracy, and effectiveness of mapping. Cartography as an important discipline among the Earth sciences has experienced technical advances with the development of programming. New methods used for spatial data processing have enabled a more effective processing of the complex datasets for modelling the Earth [28,116,117]. This enables obtaining new insights into the correlations among the Earth phenomena. This increases the possibilities of the traditional GIS used for mapping spatial data [118,119].

GIS-based mapping is used for integrated thematic maps or in risk assessment studies [120,121]. Geological GIS-based mapping is largely supported by visualisation of the provinces and units [122], statistical graphs, and plotting for hydrocarbon resource analysis [123]. Other approaches include geophysical and geochemical data analysis [124–126] or gravimetric geoid modelling [127]. The existing GIS applications of mapping Bolivia are presented in studies of the ecosystem services combining quantitative and qualitative data and spatial GIS to assess the environmental changes [128]. In contrast to the thematic applications of GIS specifically for Bolivia, using scripting techniques was presented as a special opportunity of machine-based cartography. Specifically, the scripting approach provides advantages in Earth studies in geological, geophysical, and geotechnical modelling of soil data, seismic analysis and simulation, and risk mitigation and vulnerability assessment [67–69,105,129]. The advantages of scripts can be explained by the increased speed of data processing and the accurate plotting and machine-based workflow routine, which significantly minimises man-made errors and misprints. These include such improvements as automated mapping, precise data handling, automated re-projecting, or processing big data.

This paper contributes to the increase of the geographic knowledge of Bolivia by presenting an integrated framework of the geological, topographic, seismic, and geophysical data processing by means of GIS and GMT. Specifically, it demonstrated that using scripts enables meeting the high demands of contemporary cartography, e.g., spatial analysis, computing, and visualisation of the multi-format data for an integrated analysis. A structured analysis of the data was performed to incorporate the insights into the geologic analysis using regional characteristics of lithology and geological provinces and basins of Bolivia, a special, unique region of the Central Andes, South America.

Funding: This research received no external funding.

Institutional Review Board Statement: Not applicable.

Informed Consent Statement: Not applicable.

Data Availability Statement: The GitHub repository of the author with available GMT scripts: https://github.com/paulinelemenkova/Mapping_Bolivia_GMT_Scripts (accessed on 31 May 2022).

Acknowledgments: The author gratefully acknowledges three anonymous referees who provided helpful comments and constructive suggestions on earlier drafts of the manuscript.

Conflicts of Interest: The author declares no conflict of interest.

Abbreviations

The following abbreviations are used in this manuscript:

CSV	Comma-Separated Values
EGM	Earth Gravitational Model
EGM2008	Earth Gravitational Models of 2008
GEBCO	The General Bathymetric Chart of the Oceans
GIS	Geographic Information System
GMT	Generic Mapping Tools
QGIS	Quantum GIS
IRIS	Incorporated Research Institutions for Seismology
NGA	National Geospatial-Intelligence Agency
NGDC	National Geophysical Data Center
NOAA	National Oceanic and Atmospheric Administration
SIO	Scripps Institution of Oceanography
SRTM	Shuttle Radar Topography Mission
USGS	United States Geological Survey

References

1. Chen, C.; Judge, J.; Hulse, D. PyLUSAT: An open-source Python toolkit for GIS-based land use suitability analysis. *Environ. Model. Softw.* **2022**, *151*, 105362. [CrossRef]
2. Ortolano, G.; Visalli, R.; Godard, G.; Cirrincione, R. Quantitative X-ray Map Analyser (Q-XRMA): A new GIS-based statistical approach to Mineral Image Analysis. *Comput. Geosci.* **2018**, *115*, 56–65. [CrossRef]
3. Lemenkova, P. Console-Based Mapping of Mongolia Using GMT Cartographic Scripting Toolset for Processing TerraClimate Data. *Geosciences* **2022**, *12*, 140. [CrossRef]
4. Omran, A.; Dietrich, S.; Abouelmagd, A.; Michael, M. New ArcGIS tools developed for stream network extraction and basin delineations using Python and java script. *Comput. Geosci.* **2016**, *94*, 140–149. [CrossRef]
5. Cadieux, N.; Kalacska, M.; Coomes, O.T.; Tanaka, M.; Takasaki, Y. A Python Algorithm for Shortest-Path River Network Distance Calculations Considering River Flow Direction. *Data* **2020**, *5*, 8. [CrossRef]
6. Lei, Y.; Tong, X.; Zhang, Y.; Qiu, C.; Wu, X.; Lai, G.; Li, H.; Guo, C.; Zhang, Y. Global multi-scale grid integer coding and spatial indexing: A novel approach for big earth observation data. *ISPRS J. Photogramm. Remote Sens.* **2020**, *163*, 202–213. [CrossRef]
7. Xia, J.; Yang, C.; Li, Q. Building a spatiotemporal index for Earth Observation Big Data. *Int. J. Appl. Earth Obs. Geoinf.* **2018**, *73*, 245–252. [CrossRef]
8. Nativi, S.; Mazzetti, P.; Santoro, M.; Papeschi, F.; Craglia, M.; Ochiai, O. Big Data challenges in building the Global Earth Observation System of Systems. *Environ. Model. Softw.* **2015**, *68*, 1–26. [CrossRef]
9. Wagemann, J.; Siemen, S.; Seeger, B.; Bendix, J. Users of open Big Earth data—An analysis of the current state. *Comput. Geosci.* **2021**, *157*, 104916. [CrossRef]
10. Mori, F.; Mendicelli, A.; Falcone, G.; Acunzo, G.; Spacagna, R.L.; Naso, G.; Moscatelli, M. Ground motion prediction maps using seismic-microzonation and machine learning. *Nat. Hazards Earth Syst. Sci.* **2022**, *22*, 947–966. [CrossRef]
11. Lazar, A.; Shellito, B.A. Comparing machine learning classification schemes—A GIS approach. In Proceedings of the Fourth International Conference on Machine Learning and Applications (ICMLA'05), Los Angeles, CA, USA, 15–17 December 2005; p. 7. [CrossRef]
12. Arabameri, A.; Pal, S.C.; Rezaie, F.; Nalivan, O.A.; Chowdhuri, I.; Saha, A.; Lee, S.; Moayedi, H. Modeling groundwater potential using novel GIS-based machine-learning ensemble techniques. *J. Hydrol. Reg. Stud.* **2021**, *36*, 100848. [CrossRef]
13. Zuo, R.; Wang, J.; Yin, B. Visualization and interpretation of geochemical exploration data using GIS and machine learning methods. *Appl. Geochem.* **2021**, *134*, 105111. [CrossRef]
14. Sun, T.; Chen, F.; Zhong, L.; Liu, W.; Wang, Y. GIS-based mineral prospectivity mapping using machine learning methods: A case study from Tongling ore district, eastern China. *Ore Geol. Rev.* **2019**, *109*, 26–49. [CrossRef]
15. Buck, V.; Stäbler, F.; Mohrmann, J.; González, E.; Greinert, J. Visualising geospatial time series datasets in realtime with the Digital Earth Viewer. *Comput. Graph.* **2022**, *103*, 121–128. [CrossRef]
16. Lemenkova, P. Mapping topographic, geophysical and gravimetry data of Pakistan—A contribution to geological understanding of Sulaiman Fold Belt and Muslim Bagh Ophiolite Complex. *Geophysica* **2021**, *56*, 3–26. [CrossRef]
17. Zhao, S. Remote sensing data fusion using support vector machine. In Proceedings of the IGARSS 2004—2004 IEEE International Geoscience and Remote Sensing Symposium, Anchorage, AK, USA, 20–24 September 2004; Volume 4, pp. 2575–2578. [CrossRef]
18. Zhu, J.; Wu, P. BIM/GIS data integration from the perspective of information flow. *Autom. Constr.* **2022**, *136*, 104166. [CrossRef]
19. Kreklow, J.; Tetzlaff, B.; Kuhnt, G.; Burkhard, B. A Rainfall Data Intercomparison Dataset of RADKLIM, RADOLAN, and Rain Gauge Data for Germany. *Data* **2019**, *4*, 118. [CrossRef]
20. Devoto, S.; Hastewell, L.J.; Prampolini, M.; Furlani, S. Dataset of Gravity-Induced Landforms and Sinkholes of the Northeast Coast of Malta (Central Mediterranean Sea). *Data* **2021**, *6*, 81. [CrossRef]

21. Demir Altıntaş, Y.; Ilal, M.E. Loose coupling of GIS and BIM data models for automated compliance checking against zoning codes. *Autom. Constr.* **2021**, *128*, 103743. [CrossRef]
22. Ma, Z.; Mei, G. Deep learning for geological hazards analysis: Data, models, applications, and opportunities. *Earth-Sci. Rev.* **2021**, *223*, 103858. [CrossRef]
23. Lemenkova, P. Seismicity in the Afar Depression and Great Rift Valley, Ethiopia. *Environ. Res. Eng. Manag.* **2022**, *78*, 83–96. [CrossRef]
24. Tamiminia, H.; Salehi, B.; Mahdianpari, M.; Quackenbush, L.; Adeli, S.; Brisco, B. Google Earth Engine for geo-big data applications: A meta-analysis and systematic review. *ISPRS J. Photogramm. Remote Sens.* **2020**, *164*, 152–170. [CrossRef]
25. Mercier, A.; Betbeder, J.; Denize, J.; Roger, J.L.; Spicher, F.; Lacoux, J.; Roger, D.; Baudry, J.; Hubert-Moy, L. Estimating crop parameters using Sentinel-1 and 2 datasets and geospatial field data. *Data Brief* **2021**, *38*, 107408. [CrossRef] [PubMed]
26. Balenzano, A.; Mattia, F.; Satalino, G.; Lovergine, F.P.; Palmisano, D.; Davidson, M.W. Dataset of Sentinel-1 surface soil moisture time series at 1 km resolution over Southern Italy. *Data Brief* **2021**, *38*, 107345. [CrossRef]
27. Allenby, R.J. Origin of the Bolivian Andean orocline: A geologic study utilizing Landsat and shuttle imaging radar. *Tectonophysics* **1987**, *142*, 137–154. [CrossRef]
28. Lombardo, U.; Grützner, C. Tectonic geomorphology and active faults in the Bolivian Amazon. *Glob. Planet. Chang.* **2021**, *203*, 103544. [CrossRef]
29. Samara e Silva Medeiros, E.; Machado, C.C.C.; Galvíncio, J.D.; de Moura, M.S.B.; de Araujo, H.F.P. Data of plant diversity, spectral reflectance at specie level and satellite spectral variables from the largest dry forest nucleus in South America. *Data Brief* **2019**, *25*, 104335. [CrossRef]
30. Talib, O.C.; Shimon, W.; Sarah, K.; Tonian, R. Detection of sinkhole activity in West-Central Florida using InSAR time series observations. *Remote Sens. Environ.* **2022**, *269*, 112793. [CrossRef]
31. Li, S.; Xu, W.; Li, Z. Review of the SBAS InSAR Time-series algorithms, applications, and challenges. *Geod. Geodyn.* **2022**, *13*, 114–126. [CrossRef]
32. Neugirg, F.; Kaiser, A.; Huber, A.; Heckmann, T.; Schindewolf, M.; Schmidt, J.; Becht, M.; Haas, F. Using terrestrial LiDAR data to analyse morphodynamics on steep unvegetated slopes driven by different geomorphic processes. *CATENA* **2016**, *142*, 269–280. [CrossRef]
33. Nakao, K.; Kabeya, D.; Awaya, Y.; Yamasaki, S.; Tsuyama, I.; Yamagawa, H.; Miyamoto, K.; Araki, M.G. Assessing the regional-scale distribution of height growth of Cryptomeria japonica stands using airborne LiDAR, forest GIS database and machine learning. *For. Ecol. Manag.* **2022**, *506*, 119953. [CrossRef]
34. Szabó, S.; Deák, B.; Kovács, Z.; Kertész, Á.; Bertalan-Balázs, B. Dataset for landscape pattern analysis from a climatic perspective. *Data Brief* **2019**, *25*, 104187. [CrossRef] [PubMed]
35. Rujoiu-Mare, M.R.; Mihai, B.A. Mapping Land Cover Using Remote Sensing Data and GIS Techniques: A Case Study of Prahova Subcarpathians. *Procedia Environ. Sci.* **2016**, *32*, 244–255. [CrossRef]
36. Li, C.; Xian, G.; Zhou, Q.; Pengra, B.W. A novel automatic phenology learning (APL) method of training sample selection using multiple datasets for time-series land cover mapping. *Remote Sens. Environ.* **2021**, *266*, 112670. [CrossRef]
37. Kral, U.; Sönmez, E.C.; Reimer, F. Data description of "City boundary and urban district boundaries, Vienna, 1920". *Data Brief* **2021**, *38*, 107382. [CrossRef] [PubMed]
38. Ostafin, K.; Jasionek, M.; Kaim, D.; Miklar, A. Historical dataset of mills for Galicia in the Austro-Hungarian Empire/southern Poland from 1880 to the 1930s. *Data Brief* **2022**, *40*, 107709. [CrossRef]
39. Bratu, I.A. Digitizing maps procedure for scientific forestry administration by GIS database. Case study: Rasinari forestry administration. In Proceedings of the 2019 International Conference on ENERGY and ENVIRONMENT (CIEM), Timisoara, Romania, 17–18 October 2019; pp. 95–98. [CrossRef]
40. Waqar, M.M.; Rehman, F.; Ikram, M. Land suitability assessment for rice crop using geospatial techniques. In Proceedings of the 2013 IEEE International Geoscience and Remote Sensing Symposium—IGARSS, Melbourne, Australia, 21–26 July 2013; pp. 2844–2847. [CrossRef]
41. Gavette, P.; Page-Schmit, K. Utilizing Historic Cartography in 3D for Archaeological Prospection on Alcatraz. In Proceedings of the 2018 3rd Digital Heritage International Congress (DigitalHERITAGE) Held Jointly with 2018 24th International Conference on Virtual Systems Multimedia (VSMM 2018), San Francisco, CA, USA, 26–30 October 2018; pp. 1–4. [CrossRef]
42. Li, S.S.; Zhou, W.; Li, A.B. Image Watermark Similarity Calculation of GIS Vector Data. *Procedia Eng.* **2012**, *29*, 1331–1337. [CrossRef]
43. Koch, A.; Heipke, C. Semantically correct 2.5D GIS data—The integration of a DTM and topographic vector data. *ISPRS J. Photogramm. Remote Sens.* **2006**, *61*, 23–32. [CrossRef]
44. Li, A.B.; Li, S.S.; Lv, G.N. Disguise and Reduction Methods of GIS Vector Data Based on Difference Expansion Principle. *Procedia Eng.* **2012**, *29*, 1344–1350. [CrossRef]
45. Viana-Fons, J.; Gonzálvez-Maciá, J.; Payá, J. Development and validation in a 2D-GIS environment of a 3D shadow cast vector-based model on arbitrarily orientated and tilted surfaces. *Energy Build.* **2020**, *224*, 110258. [CrossRef]
46. Güler, C.; Beyhan, B.; Tağa, H. PolyMorph-2D: An open-source GIS plug-in for morphometric analysis of vector-based 2D polygon features. *Geomorphology* **2021**, *386*, 107755. [CrossRef]

47. Lindh, P.; Lemenkova, P. Evaluation of Different Binder Combinations of Cement, Slag and CKD for S/S Treatment of TBT Contaminated Sediments. *Acta Mech. Autom.* **2021**, *15*, 236–248. [CrossRef]
48. Lemenkova, P. Submarine tectonic geomorphology of the Pliny and Hellenic Trenches reflecting geologic evolution of the southern Greece. *Rud. Geol. Naft. Zb.* **2021**, *36*, 33–48. [CrossRef]
49. Li, K.; Chen, S.; Hu, G. Seismic labeled data expansion using variational autoencoders. *Artif. Intell. Geosci.* **2020**, *1*, 24–30. [CrossRef]
50. Lemenkov, V.; Lemenkova, P. Using TeX Markup Language for 3D and 2D Geological Plotting. *Found. Comput. Decis. Sci.* **2021**, *46*, 43–69. [CrossRef]
51. Zhou, R.; Cai, Y.; Zong, J.; Yao, X.; Yu, F.; Hu, G. Automatic fault instance segmentation based on mask propagation neural network. *Artif. Intell. Geosci.* **2020**, *1*, 31–35. [CrossRef]
52. Lemenkov, V.; Lemenkova, P. Measuring Equivalent Cohesion Ceq of the Frozen Soils by Compression Strength Using Kriolab Equipment. *Civ. Environ. Eng. Rep.* **2021**, *31*, 63–84. [CrossRef]
53. Schenke, H. General Bathymetric Chart of the Oceans (GEBCO). In *Encyclopedia of Marine Geosciences*, 1st ed.; Springer: Dordrecht, The Netherlands, 2016; pp. 268–269. [CrossRef]
54. Lemenkova, P. GEBCO Gridded Bathymetric Datasets for Mapping Japan Trench Geomorphology by Means of GMT Scripting Toolset. *Geod. Cartogr.* **2020**, *46*, 98–112. [CrossRef]
55. Pavlis, N.K.; Holmes, S.; Kenyon, S.C.; Factor, J.K. The development and evaluation of the Earth Gravitational Model 2008 (EGM2008). *J. Geophys. Res.* **2012**, *117*, B04406. [CrossRef]
56. Sandwell, D.T.; Müller, R.D.; Smith, W.H.F.; Garcia, E.; Francis, R. New global marine gravity model from CryoSat-2 and Jason-1 reveals buried tectonic structure. *Science* **2014**, *7346*, 65–67. [CrossRef]
57. Hubbard, B.E.; Crowley, J.K. Mineral mapping on the Chilean–Bolivian Altiplano using co-orbital ALI, ASTER and Hyperion imagery: Data dimensionality issues and solutions. *Remote Sens. Environ.* **2005**, *99*, 173–186. [CrossRef]
58. Suetova, I.A.; Ushakova, L.A.; Lemenkova, P. Geoinformation mapping of the Barents and Pechora Seas. *Geogr. Nat. Resour.* **2005**, *4*, 138–142. [CrossRef]
59. Lemenkova, P. Dataset compilation by GRASS GIS for thematic mapping of Antarctica: Topographic surface, ice thickness, subglacial bed elevation and sediment thickness. *Czech Polar Rep.* **2021**, *11*, 67–85. [CrossRef]
60. Klaučo, M.; Gregorová, B.; Stankov, U.; Marković, V.; Lemenkova, P. Determination of ecological significance based on geostatistical assessment: A case study from the Slovak Natura 2000 protected area. *Open Geosci.* **2013**, *5*, 28–42. [CrossRef]
61. Klauco, M.; Gregorová, B.; Koleda, P.; Stankov, U.; Markovic, V.; Lemenkova, P. Land Planning as a Support for Sustainable Development Based on Tourism: A Case Study of Slovak Rural Region. *Environ. Eng. Manag. J.* **2017**, *16*, 449–458. [CrossRef]
62. QGIS Association. *QGIS Geographic Information System*; QGIS Association: 2021. Available online: https://www.qgis.org/en/site/about/index.html (accessed on 14 April 2022).
63. Wessel, P.; Luis, J.F.; Uieda, L.; Scharroo, R.; Wobbe, F.; Smith, W.H.F.; Tian, D. The Generic Mapping Tools version 6. *Geochem. Geophys. Geosyst.* **2019**, *20*, 5556–5564. [CrossRef]
64. Gauger, S.; Kuhn, G.; Gohl, K.; Feigl, T.; Lemenkova, P.; Hillenbrand, C. Swath-bathymetric mapping. *Rep. Polar Mar. Res.* **2007**, *557*, 38–45. [CrossRef]
65. Lemenkova, P. Variations in the bathymetry and bottom morphology of the Izu-Bonin Trench modelled by GMT. *Bull. Geogr. Phys. Geogr. Ser.* **2020**, *18*, 41–60. [CrossRef]
66. Lemenkova, P. Geophysical Mapping of Ghana Using Advanced Cartographic Tool GMT. *Kartogr. Geoinf.* **2021**, *20*, 16–37. [CrossRef]
67. Falcone, G.; Acunzo, G.; Mendicelli, A.; Mori, F.; Naso, G.; Peronace, E.; Porchia, A.; Romagnoli, G.; Tarquini, E.; Moscatelli, M. Seismic amplification maps of Italy based on site-specific microzonation dataset and one-dimensional numerical approach. *Eng. Geol.* **2021**, *289*, 106170. [CrossRef]
68. Jiang, C.; Yahong, D.; Huangdong, M.; You, X.; Ge, C. A microtremor study to reveal the dynamic response of earth fissure site: the case study in Fenwei Basins, China. *Environ. Earth Sci.* **2022**, *81*, 80. [CrossRef]
69. Fayjaloun, R.; Negulescu, C.; Roullé, A.; Auclair, S.; Gehl, P.; Faravelli, M. Sensitivity of Earthquake Damage Estimation to the Input Data (Soil Characterization Maps and Building Exposure): Case Study in the Luchon Valley, France. *Geosciences* **2021**, *11*, 249. [CrossRef]
70. Anderson, R.B.; Long, S.P.; Horton, B.K.; Calle, A.Z.; Soignard, E. Late Paleozoic Gondwanide deformation in the Central Andes: Insights from RSCM thermometry and thermal modeling, southern Bolivia. *Gondwana Res.* **2021**, *94*, 222–242. [CrossRef]
71. Arguedas, J.D. *Alcide d'Orbigny: Estudios Sobre la Geología de Bolivia. El Naturalista Francés Alcide Dessaline d'Orbigny en la Visión de los Bolivianos*; Institut Français d'Études Andines: Lima, Peru, 2002; pp. 195–210. [CrossRef]
72. Forbes, D. On the Geology of Bolivia and Southern Peru. *Q. J. Geol. Soc.* **1861**, *17*, 7–62. [CrossRef]
73. Suárez Soruco, R. *Compendio de Geología de Bolivia*; Revista Técnica de Yacimientos Petrolíferos Fiscales Bolivianos: Cochabamba, Bolivia, 2000; Volume 18.
74. Ahfeld, F.; Branisa, L. *Geologia de Bolivia*; Instituto Boliviano del Petroleo, Editorial Don Bosco: La Paz, Bolivia, 1960.
75. Allenby, R.J. Origin of rectangular and aligned lakes in the Beni Basin of Bolivia. *Tectonophysics* **1988**, *145*, 1–20. [CrossRef]
76. Ramos, V.A. Fifty years of plate tectonics in the Central Andes. *J. S. Am. Earth Sci.* **2021**, *105*, 102997. [CrossRef]

77. Fernandez, G.A.; Assumpção, M.; Nieto, M.; Griffiths, T.; Convers, J. Focal mechanism of the 5.1Mw 2014 Lloja earthquake, Bolivia: Probing the transition between extensional stresses of the central Altiplano and compressional stresses of the sub-Andes. *J. S. Am. Earth Sci.* **2019**, *91*, 102–107. [CrossRef]
78. Funning, G.J.; Barke, R.M.D.; Lamb, S.H.; Minaya, E.; Parsons, B.; Wright, T.J. The 1998 Aiquile, Bolivia earthquake: A seismically active fault revealed with InSAR. *Earth Planet. Sci. Lett.* **2005**, *232*, 39–49. [CrossRef]
79. Lima, I.Q.; Muñoz, M.O.; Ramos Ramos, O.E.; Aguirre, J.Q.; Maity, J.P.; Ahmad, A.; Bhattacharya, P. Hydrogeochemical contrasts in the shallow aquifer systems of the Lower Katari Basin and Southern Poopó Basin, Bolivian Altiplano. *J. S. Am. Earth Sci.* **2021**, *105*, 102914. [CrossRef]
80. Lima, I.Q.; Ramos Ramos, O.E.; Muñoz, M.O.; Chambi Tapia, M.I.; Aguirre, J.Q.; Ahmad, A.; Maity, J.P.; Islam, M.; Prosun Bhattacharya, T. Geochemical mechanisms of natural arsenic mobility in the hydrogeologic system of Lower Katari Basin, Bolivian Altiplano. *J. Hydrol.* **2021**, *594*, 125778. [CrossRef]
81. Avilés, G.P.F.; Descloitres, M.; Duwig, C.; Rossier, Y.; Spadini, L.; Legchenko, A.; Soruco, A.; Argollo, J.; Pérez, M.; Medinaceli, W. Insight into the Katari-Lago Menor Basin aquifer, Lake Titicaca-Bolivia, inferred from geophysical (TDEM), hydrogeological and geochemical data. *J. S. Am. Earth Sci.* **2020**, *99*, 102479. [CrossRef]
82. Borsa, A.A.; Fricker, H.A.; Bills, B.G.; Minster, J.B.; Carabajal, C.C.; Quinn, K.J. Topography of the salar de Uyuni, Bolivia from kinematic GPS. *Geophys. J. Int.* **2008**, *172*, 31–40. [CrossRef]
83. Dorbath, C.; Granet, M. Local earthquake tomography of the Altiplano and the Eastern Cordillera of northern Bolivia. *Tectonophysics* **1996**, *259*, 117–136. [CrossRef]
84. Dahm, T.; Krüger, F. Higher-degree moment tensor inversion using far-field broad-band recordings: Theory and evaluation of the method with application to the 1994 Bolivia deep earthquake. *Geophys. J. Int.* **1999**, *137*, 35–50. [CrossRef]
85. Boger, S.D.; Raetz, M.; Giles, D.; Etchart, E.; Fanning, C.M. U-Pb age from the Sunsás region of Eastern Bolivia, evidence for allochthonous origin of the Paraguá Block. *Precambrian Res.* **2005**, *139*, 121–146. [CrossRef]
86. Redwood, S.D.; Rice, C.M. Petrogenesis of Miocene basic shoshonitic lavas in the Bolivian Andes and implications for hydrothermal gold, silver and tin deposits. *J. S. Am. Earth Sci.* **1997**, *10*, 203–221. [CrossRef]
87. Iqbal, B.A. The economics of tin mining in Bolivia: By M. A. Ayub World Bank, Washington, DC, 1985. *Resour. Policy* **1986**, *12*, 153–154. [CrossRef]
88. Diaz-Cuellar, V. The political economy of mining in Bolivia during the government of the Movement Towards Socialism (2006–2015). *Extr. Ind. Soc.* **2017**, *4*, 120–130. [CrossRef]
89. Guédron, S.; Tolu, J.; Delaere, C.; Sabatier, P.; Barre, J.; Heredia, C.; Brisset, E.; Campillo, S.; Bindler, R.; Fritz, S.C.; et al. Reconstructing two millennia of copper and silver metallurgy in the Lake Titicaca region (Bolivia/Peru) using trace metals and lead isotopic composition. *Anthropocene* **2021**, *34*, 100288. [CrossRef]
90. Pavilonis, B.; Grassman, J.; Johnson, G.; Diaz, Y.; Caravanos, J. Characterization and risk of exposure to elements from artisanal gold mining operations in the Bolivian Andes. *Environ. Res.* **2017**, *154*, 1–9. [CrossRef]
91. Narins, T.P. The battery business: Lithium availability and the growth of the global electric car industry. *Extr. Ind. Soc.* **2017**, *4*, 321–328. [CrossRef]
92. Sanchez-Lopez, M.D. Territory and lithium extraction: The Great Land of Lipez and the Uyuni Salt Flat in Bolivia. *Political Geogr.* **2021**, *90*, 102456. [CrossRef]
93. Plotzki, A.; May, J.H.; Preusser, F.; Roesti, B.; Denier, S.; Lombardo, U.; Veit, H. Geomorphology and evolution of the late Pleistocene to Holocene fluvial system in the south-eastern Llanos de Moxos, Bolivian Amazon. *CATENA* **2015**, *127*, 102–115. [CrossRef]
94. Dumont, J.F.; Fournier, M. Geodynamic environment of Quaternary morphostructures of the subandean foreland basins of Peru and Bolivia: Characteristics and study methods. *Quat. Int.* **1994**, *21*, 129–142. [CrossRef]
95. May, J.H. Dunes and dunefields in the Bolivian Chaco as potential records of environmental change. *Aeolian Res.* **2013**, *10*, 89–102. [CrossRef]
96. Baumann, M.; Levers, C.; Macchi, L.; Bluhm, H.; Waske, B.; Gasparri, N.I.; Kuemmerle, T. Mapping continuous fields of tree and shrub cover across the Gran Chaco using Landsat 8 and Sentinel-1 data. *Remote Sens. Environ.* **2018**, *216*, 201–211. [CrossRef]
97. Thomas, E.; Semo, L.; Morales, M.; Noza, Z.; Nuñez, H.; Cayuba, A.; Noza, M.; Humaday, N.; Vaya, J.; Van Damme, P. Ethnomedicinal practices and medicinal plant knowledge of the Yuracarés and Trinitarios from Indigenous Territory and National Park Isiboro-Sécure, Bolivian Amazon. *J. Ethnopharmacol.* **2011**, *133*, 153–163. [CrossRef]
98. Burbridge, R.E.; Mayle, F.E.; Killeen, T.J. Fifty-thousand-year vegetation and climate history of Noel Kempff Mercado National Park, Bolivian Amazon. *Quat. Res.* **2004**, *61*, 215–230. [CrossRef]
99. Cadima, X.; Van Zonneveld, M.; Scheldeman, X.; Castañeda, N.; Patiño, F.; Beltran, M.; Van Damme, P. Endemic wild potato (*Solanum* spp.) biodiversity status in Bolivia: Reasons for conservation concerns. *J. Nat. Conserv.* **2014**, *22*, 113–131. [CrossRef]
100. Capriles, J.M.; Albarracin-Jordan, J. The earliest human occupations in Bolivia: A review of the archaeological evidence. *Quat. Int.* **2013**, *301*, 46–59. [CrossRef]
101. Rivadeneyra-Vera, C.; Assumpção, M.; Minaya, E.; Aliaga, P.; Avila, G. Determination of the fault plane and rupture size of the 2013 Santa Cruz earthquake, Bolivia, 5.2 Mw, by relative location of the aftershocks. *J. S. Am. Earth Sci.* **2016**, *71*, 54–62. [CrossRef]
102. Tono, Y.; Yomogida, K. Origin of short-period signals following P-diffracted waves: A case study of the 1994 Bolivian deep earthquake. *Phys. Earth Planet. Inter.* **1997**, *103*, 1–16. [CrossRef]

103. González-Maurel, O.; Deegan, F.M.; Le Roux, P.; Harris, C.; Troll, V.R.; Godoy, B. Constraining the sub-arc, parental magma composition for the giant Altiplano-Puna Volcanic Complex, northern Chile. *Sci. Rep.* **2020**, *10*, 6864. [CrossRef] [PubMed]
104. Lemenkova, P. Geomorphological modelling and mapping of the Peru-Chile Trench by GMT. *Pol. Cartogr. Rev.* **2019**, *51*, 181–194. [CrossRef]
105. Petersen, M.D.; Harmsen, S.C.; Jaiswal, K.S.; Rukstales, K.S.; Luco, N.; Haller, K.M.; Mueller, C.S.; Shumway, A.M. Seismic Hazard, Risk, and Design for South America. *Bull. Seismol. Soc. Am.* **2018**, *108*, 781–800. [CrossRef]
106. Barone, A.; Fedi, M.; Tizzani, P.; Castaldo, R. Multiscale Analysis of DInSAR Measurements for Multi-Source Investigation at Uturuncu Volcano (Bolivia). *Remote Sens.* **2019**, *11*, 703. [CrossRef]
107. Zhu, L. Recovering permanent displacements from seismic records of the June 9, 1994 Bolivia deep earthquake. *Geophys. Res. Lett.* **2003**, *30*, 1740. [CrossRef]
108. Ekström, G. Calculation of static deformation following the Bolivia Earthquake by summation of Earth's normal modes. *Geophys. Res. Lett.* **1995**, *22*, 2289–2292. [CrossRef]
109. Heine, K. Late Quaternary glaciations of Bolivia. In *Developments in Quaternary Sciences*; Elsevier: Amsterdam, The Netherlands, 2004; Volume 2, Chapter Part C, pp. 83–88. [CrossRef]
110. La Frenierre, J.; Huh, K.; Mark, B.G. Ecuador, Peru and Bolivia. In *Quaternary Glaciations—Extent and Chronology: A Closer Look*; Elsevier: Amsterdam, The Netherlands, 2011; Volume 15.
111. Latrubesse, E.M.; Baker, P.A.; Argollo, J. Geomorphology of Natural Hazards and Human-induced Disasters in Bolivia. *Dev. Earth Surf. Process.* **2009**, *13*, 181–194. [CrossRef]
112. Latrubesse, E.M.; Stevaux, J.C.; Cremon, E.H.; May, J.H.; Tatumi, S.H.; Hurtado, M.A.; Bezada, M.; Argollo, J.B. Late Quaternary megafans, fans and fluvio-aeolian interactions in the Bolivian Chaco, Tropical South America. *Palaeogeogr. Palaeoclimatol. Palaeoecol.* **2012**, *356–357*, 75–88. [CrossRef]
113. May, J.H.; Argollo, J.; Veit, H. Holocene landscape evolution along the Andean piedmont, Bolivian Chaco. *Palaeogeogr. Palaeoclimatol. Palaeoecol.* **2008**, *260*, 505–520. [CrossRef]
114. Holder, R.M.; Viete, D.R.; Brown, M.; Johnson, T.E. Metamorphism and the evolution of plate tectonics. *Nature* **2019**, *572*, 378–381. [CrossRef] [PubMed]
115. Tapia, J.; Murray, J.; Ormachea, M.; Tirado, N.; Nordstrom, D.K. Origin, distribution, and geochemistry of arsenic in the Altiplano-Puna plateau of Argentina, Bolivia, Chile, and Perú. *Sci. Total. Environ.* **2019**, *678*, 309–325. [CrossRef] [PubMed]
116. Bar, N.; Long, M.D.; Wagner, L.S.; Beck, S.L.; Zandt, G.; Tavera, H. Receiver function analysis reveals layered anisotropy in the crust and upper mantle beneath southern Peru and northern Bolivia. *Tectonophysics* **2019**, *753*, 93–110. [CrossRef]
117. Lemenkova, P. GRASS GIS for topographic and geophysical mapping of the Peru-Chile Trench. *Forum Geogr.* **2020**, *19*, 143–157. [CrossRef]
118. Millington, A.C.; Velez-Liendo, X.M.; Bradley, A.V. Scale dependence in multitemporal mapping of forest fragmentation in Bolivia: Implications for explaining temporal trends in landscape ecology and applications to biodiversity conservation. *ISPRS J. Photogramm. Remote. Sens.* **2003**, *57*, 289–299. [CrossRef]
119. Lemenkova, P. Evaluating land cover types from Landsat TM using SAGA GIS for vegetation mapping based on ISODATA and K-means clustering. *Acta Agric. Serbica* **2021**, *26*, 159–165. [CrossRef]
120. Vella, M.A.; Loget, N. Geomorphological map of the Tiwanaku River watershed in Bolivia: Implications for past and present human occupation. *CATENA* **2021**, *206*, 105508. [CrossRef]
121. Lemenkova, P. Scripting cartographic techniques of R and GMT for geomorphological and topographic mapping of Peru. *Entorno Geogr.* **2021**, *22*, 36–55. [CrossRef]
122. Nedel, I.M.; Fuck, R.A.; Ruiz, A.S.; Matos-Salinas, G.R.; Da C. D. Ferreira, A. Timing of Proterozoic magmatism in the Sunsas belt, Bolivian Precambrian Shield, SW Amazonian Craton. *Geosci. Front.* **2021**, *12*, 101247. [CrossRef]
123. Jemio, L.C. *Booms and Collapses of the Hydro Carbons Sector in Bolivia*; Institute for Advanced Development Studies: La Paz, Bolivia, 2008.
124. Collinson, D.W. Magnetic Properties of the Taiguati Formation, Bolivia. *Geophys. J. Int.* **1966**, *11*, 337–347. [CrossRef]
125. Lindh, P.; Lemenkova, P. Geochemical tests to study the effects of cement ratio on potassium and TBT leaching and the pH of the marine sediments from the Kattegat Strait, Port of Gothenburg, Sweden. *Baltica* **2022**, *35*, 47–59. [CrossRef]
126. Ocola, L.C.; Meyer, R.P. Crustal Low-Velocity Zones Under the Peru-Bolivia Altiplano. *Geophys. J. Int.* **1972**, *30*, 199–208. [CrossRef]
127. Corchete, V.; Flores, D.; Oviedo, F. The first high-resolution gravimetric geoid for the Bolivian tableland: BOLGEO. *Phys. Earth Planet. Inter.* **2006**, *157*, 250–256. [CrossRef]
128. Hinojosa, L.; Hennermann, K. A GIS approach to ecosystem services and rural territorial dynamics applied to the case of the gas industry in Bolivia. *Appl. Geogr.* **2012**, *34*, 487–497. [CrossRef]
129. Lindh, P.; Lemenkova, P. Resonant Frequency Ultrasonic P-Waves for Evaluating Uniaxial Compressive Strength of the Stabilized Slag–Cement Sediments. *Nord. Concr. Res.* **2021**, *65*, 39–62. [CrossRef]